Shock and Vibration 11 (2004) 281–293
IOS Press

Identification of the 3D vibratory motion of a rigid body by accelerometer measurements

Francesca Di Puccio* and Paola Forte
Department of Mechanical, Nuclear and Production Engineering, University of Pisa, Italy

This paper is dedicated to Prof.Piombo, for his fundamental work in the field of the analysis of vibrations.

Abstract. The identification of the motion of a rigid body by means of linear accelerometers is a problem already investigated by many researchers, but still debated. The optimisation of the number and placement of accelerometers is also another important aspect of the problem. In this study, an experimental procedure is proposed and applied to identify the rigid-body vibratory motion of the steering wheel of a sporting car, by means of six linear accelerometers. Some numerical simulations for investigating possible errors are also presented.

Keywords: Accelerometer, rigid motion, vibrations, kinematics

1. Introduction

The use of accelerometers for the determination of the rigid-body motion, although apparently a classical and elementary application, is still far from being standardised especially for what concerns the number and placement of the accelerometers.

It can be shown that in theory six properly placed linear accelerometers are necessary for a complete definition of the rigid body motion. The six accelerometer scheme presented in [4] requires the numerical integration of three non linear differential equations in terms of angular acceleration components and cross-products of the angular velocity components, meaning an accumulation of error. So, especially in those cases where high accelerations are involved, such as in impact, the accuracy obtained is not satisfactory. Moreover there is a question of stability of the solution [2] which is not simple to prove. Therefore a nine accelerometer scheme is proposed [4] to determine angular acceleration components only by the linear acceleration values while the angular velocity components are obtained by simple integration.

In order to determine the unique solution of the system of equations in the three unknown vectors – linear acceleration, angular acceleration and angular velocity –, avoiding integrations and knowledge of the initial state, at least twelve properly placed and oriented linear accelerometers should be used [5,6]. The redundancy of the system is used to eliminate singularities and indeterminants due to the presence of quadratic terms and cross-products of angular velocity components.

However, the use of twelve linear accelerometers or four triaxial ones requires that the instrumented body has four properly oriented and sufficiently large plane areas where the sensors can be fixed. Practically, though, if the body is small and not a lab prototype then this is a difficult requirement. Moreover a twelve channel DAQ system for simultaneous acquisition is rather costly. On the other hand if high precision, low sensitivity accelerometers are available, data acquisition is accurate, and if low accelerations are involved, the six accelerometer scheme is shown to work [4]. A calibration procedure can be followed to reduce misalignment as suggested in [5].

*Corresponding author: Francesca Di Puccio, Dipartimento di Ingegneria Meccanica, Nucleare e della Produzione, via Diotisalvi 2, 56126 Pisa, Italy. Fax: +39 50 836665; E-mail: dipuccio@ing. unipi.it.

ISSN 1070-9622/04/$17.00

While the problem of determining rigid-body angular velocity in a mobile frame by means of a suitable number of accelerometers has been considered, an aspect somehow neglected in the previous papers, is the calculation of rigid-body orientation relative to an inertially fixed frame. A method based on the orientation vector concept is formulated and tested in [3] and is found to be suitable for the accelerometer data.

In this study, we propose a procedure for the application of six linear accelerometers to determine the small vibrations of a rigid body. The peculiarity of considering small vibrations is fundamental for transferring the acceleration components from a body fixed reference frame (BRF) to an inertial reference frame (IRF).

The procedure was verified on the steering wheel of a sporting car. The hub rigid-body motion during the car ride was used as a cheap 3D exciting source for the steering wheel. Accelerometer measurements on the wheel ring joined with a harmonic FE analysis made identification of the steering wheel modal characteristics possible [1].

2. Basic equations

As it is well known from Theoretical Mechanics, a fundamental relationship exists between the velocities of two points, P and O, of a rigid body

$$\boldsymbol{\nu}_P = \boldsymbol{\nu}_O + \boldsymbol{\omega} \times (P - O) \tag{1}$$

where $\boldsymbol{\omega}$ is the body angular velocity.

A similar relationship for accelerations is given by Rival's Theorem

$$\boldsymbol{a}_P = \boldsymbol{a}_O + \dot{\boldsymbol{\omega}} \times (P - O) + \boldsymbol{\omega} \times [\boldsymbol{\omega} \times (P - O)] \tag{2}$$

where $\dot{\boldsymbol{\omega}}$ is the angular acceleration.

From Eqs (1) and (2), it is evident that to completely describe the rigid-body kinematics, 12 scalar quantities, that is the components of $\boldsymbol{\nu}_O$, $\boldsymbol{a}_O, \boldsymbol{\omega}$ and $\dot{\boldsymbol{\omega}}$, are required, the acceleration state alone requiring the latter three vectors. The corresponding 9 scalar components are obtained on the basis of accelerometer measurements, while additional information about the linear velocity $\boldsymbol{\nu}_o$ has to be obtained from different measurements or considerations.

Moreover it is worth noting that accelerometers give measurements (components) in a BRF, requiring careful data processing, as shown in the next paragraph. In fact the afore-mentioned fundamental Eqs (1–2) can be expressed both in an IRF and in a BRF

$$[\boldsymbol{\nu}_P] = [\boldsymbol{\nu}_O] + [\boldsymbol{\omega}] \times [P - O] \tag{1a}$$

$$[\boldsymbol{a}_P] = [\boldsymbol{a}_O] + [\dot{\boldsymbol{\omega}}] \times [P - O] + [\boldsymbol{\omega}] \times ([\boldsymbol{\omega}] \times [P - O]) \tag{2a}$$

where each vector in square brackets means its components in the specified frame, e.g. $[P - O]_I$ and $[P - O]_B$ respectively for components in IRF and BRF. The main difference in the two reference systems is that $[P - O]_I$ is time dependent while $[P - O]_B$ is a constant vector, since both P and O belong to the body.

Another important difference is that, while in the IRF Eq. (2a) comes directly from the derivative of Eq. (1a) due to the relation

$$\left[\frac{d\mathbf{w}}{dt}\right]_I = \frac{d}{dt}[\mathbf{w}]_I \tag{3}$$

which holds for a generic vector **w**, for the mobile frame BRF there is an additional term. In fact in a mobile frame, the angular velocity of the frame itself, which in this case is also equal to the body angular velocity $\boldsymbol{\omega}$, has to be taken into account, yielding the following expression

$$\left[\frac{d\mathbf{w}}{dt}\right]_B = \frac{d}{dt}[\mathbf{w}]_B + [\boldsymbol{\omega}]_B \times [\mathbf{w}]_B. \tag{4}$$

This difference is important when treating accelerometric data, because experimental measurements give $[\boldsymbol{a}]_B$, that, according to Eq. (4), can be written as

$$[\boldsymbol{a}]_B = \left[\frac{d\boldsymbol{\nu}}{dt}\right]_B = \frac{d}{dt}[\boldsymbol{\nu}]_B + [\boldsymbol{\omega}]_B \times [\boldsymbol{\nu}]_B. \tag{5}$$

Thus it is not possible to simply integrate accelerometric data to obtain linear velocity, but it is necessary to solve differential Eq. (5).

A further step may require to transfer all accelerometric data in an IRF, e.g. by means of gyroscopes, image-based techniques or other methods such as that described in [3].

However, in some particular case as for small vibrations, both the integration of accelerometric data and the change of reference frame can be simplified.

2.1. Vibratory motion

One of the main fields of accelerometer applications, especially as far as mechanical systems are concerned, is related to vibrations.

For small vibrations, it is commonly assumed that the position of one point can be expressed by means of a simple trigonometric expression for each component

$$P - P_0 = \begin{bmatrix} \sum_{i=1}^{n} lx_{Pi} \cos(\overline{\omega}_i t + \varphi x_i) \\ \sum_{i=1}^{n} ly_{Pi} \cos(\overline{\omega}_i t + \varphi y_i) \\ \sum_{i=1}^{n} lz_{Pi} \cos(\overline{\omega}_i t + \varphi z_i) \end{bmatrix}$$

P_0 corresponding to the equilibrium position, $\overline{\omega}_i$ being the pulsation, $\varphi x_i, \varphi y_i, \varphi z_i$ the phase angles and $lx_{pi}, ly_{pi}, lz_{pi}$ the amplitudes. A more compact form for the above equation is introduced

$$P - P_0 = \sum_{i=1}^{n} \overline{\boldsymbol{l}}_{Pi} \cos(\overline{\omega}_i t + \boldsymbol{\varphi}_i) \tag{6}$$

in terms of phase and amplitude vectors, $\boldsymbol{\varphi}_i$ and $\overline{\boldsymbol{l}}_{Pi}$. If the above expression is defined in an IRF, the following relationships hold

$$\boldsymbol{\nu}_P = \sum_{i=1}^{n} \overline{\boldsymbol{\nu}}_{Pi} \sin(\overline{\omega}_i t + \boldsymbol{\varphi}_i) \tag{7}$$

$$\boldsymbol{a}_P = \sum_{i=1}^{n} \overline{\boldsymbol{a}}_{Pi} \cos(\overline{\omega}_i t + \boldsymbol{\varphi}_i) \tag{8}$$

$$\overline{\boldsymbol{a}}_{Pi} = \overline{\omega}_i \overline{\boldsymbol{\nu}}_{Pi} = \overline{\omega}_i^2 \overline{\boldsymbol{l}}_{Pi} \tag{9}$$

where $\overline{\boldsymbol{\nu}}_{Pi}$ and $\overline{\boldsymbol{a}}_{Pi}$ are the amplitude vectors.

The trigonometric form in Eqs (6–8) is useful when treating experimental data, since it is can be easily compared with the corresponding FFT. In case of accelerometric data the FFT should be done after a change of reference system from BRF to IRF, if the orientation of the body is known. For small vibrations this step can be avoided, since in general

$$[\boldsymbol{w}]_I \approx [\boldsymbol{w}]_B \rightarrow [\boldsymbol{a}_P]_I \approx [\boldsymbol{a}_P]_B. \tag{10}$$

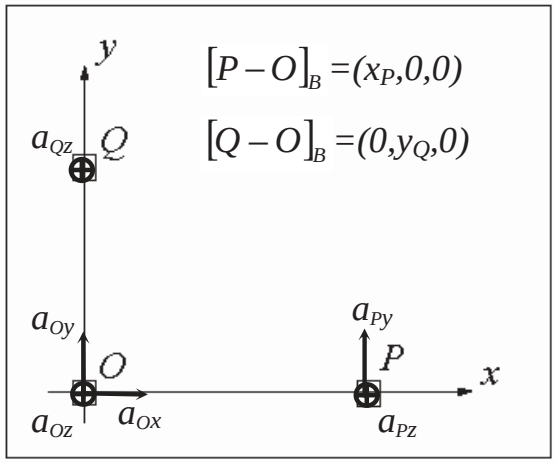

Fig. 1. Placement of the accelerometers.

2.2. Accelerometric data processing

According to the previous theoretical foundations, a procedure can be defined in order to employ linear accelerometers to determine the motion of a vibrating rigid-body.

We can consider that for each accelerometer, it is possible to obtain the FFT of the acceleration ($\overline{\omega}_i, \overline{\boldsymbol{a}}_{Pi}$ and $\boldsymbol{\varphi}_i$) and, by Eqs (7–9), also the velocity of each point. Once the velocities are determined, it is possible to get the three components of the body angular velocity from Eq. (1). That means that six linear velocity components must have been previously determined by as many accelerometer measurements. It is worth noting that in addition to O and P, a third point Q of the body, must be considered, since from Eq. (1) the component of $\boldsymbol{\omega}$ parallel to $P - O$ cannot be evaluated. Finally it is convenient to consider $\boldsymbol{\nu}_O$, two components of $\boldsymbol{\nu}_P$ and one of $\boldsymbol{\nu}_Q$. A suitable placement of the accelerometers is described in Fig. 1 where the three points are indicated together with the corresponding acquired quantities:

– a triaxial accelerometer in O (a_{Ox}, a_{Oy}, a_{Oz})
– a biaxial accelerometer in $P(a_{Py}, a_{Pz})$
– a linear accelerometer in $Q, (a_{Qz})$.

A BRF is assumed, with the x-axis along $O - P$ and the y-axis along $O - Q$.

The expressions that give the components of the angular velocity are

$$\omega_x = \frac{\nu_{Qz} - \nu_{Oz}}{y_Q} \tag{11}$$

$$\omega_y = \frac{\nu_{Pz} - \nu_{Oz}}{x_P} \tag{12}$$

$$\omega_z = \frac{\nu_{Py} - \nu_{Oy}}{x_P} \tag{13}$$

The calculation of the angular acceleration $\dot{\boldsymbol{\omega}}$ can be carried out in a similar way, once the angular velocity has been determined

$$\dot{\boldsymbol{\omega}}_x = \frac{a_{Qz} - a_{Oz}}{y_Q} - \omega_y \omega_z \tag{14}$$

$$\dot{\boldsymbol{\omega}}_y = \frac{a_{Pz} - a_{Oz}}{x_P} - \omega_x \omega_z \tag{15}$$

$$\dot{\boldsymbol{\omega}}_z = \frac{a_{Py} - a_{Oy}}{x_P} - \omega_x \omega_y \tag{16}$$

In this way only six measurements are needed to determine the vibratory motion of a rigid body.

3. Numerical simulation

The above procedure has been used both in numerical simulations and in a real experiment.

Let us consider a small angular oscillation $\theta(t)$

$$\theta(t) = \Theta \cos(\overline{\omega} t + \psi) \tag{17}$$

about an axis passing through the origin Ω of the IRF (which is not necessarily coincident with O), and characterised by a unit vector $\boldsymbol{n}$

$$\boldsymbol{n} = (\cos\beta \sin\alpha, \sin\beta \sin\alpha, \cos\alpha). \tag{18}$$

The rotation matrix describing this oscillation is given by the product of 5 elemental matrices

$$R(t) = R_z(\alpha) R_y(\beta) R_z(\theta(t)) R_y(-\beta) R_z(-\alpha) \tag{19}$$

and can be also used to transform vectors from a BRF to the IRF.

By means of a simple Mathcad worksheet the effects of some experimental errors related to:

a) accelerometer location
b) orientation of accelerometer axes
c) and IRF vs. BRF components

have been analysed.

3.1. Accelerometer location

An error in evaluating the BRF components of the position vectors of the accelerometers ($[P-O]_B$ and $[Q-O]_B$) has been considered and expressed as a percentage of the accelerometer maximum dimension in the $x-y$ plane ($l = 10$ mm). This reference length has been chosen as representative of the scale of the problem. The influence of the accelerometer location error has been investigated for different distances between the accelerometers themselves and the rotation axis and for different orientations of the vector $\boldsymbol{n}$.

The worst condition occurs when O belongs to the rotation axis and the distance between the point P/Q and O is of the same order of the accelerometer dimension l, i.e. $|x_p| \approx l$ and $|y_Q| \approx l$. In this case the error in the location means the same error in the acceleration. This error decreases as $|x_p|$ and $|y_Q|$ grow.

As the distance of O from the rotation axis increases, the error in the position of the accelerometers becomes less and less important. For example when this distance is 10 l and $x_p = y_Q = l$, an error of 5% in the position yields an error of only 0.5% in the acceleration, independent of the oscillation amplitude and pulsation, and of the orientation of $\boldsymbol{n}$.

3.2. Orientation of accelerometer axes

Another error that can occur in the set up of accelerometers is a misalignment of their axes. Some simulations have been carried out in order to estimate the importance of such errors. An undesired rotation has been imposed to the accelerometer axes in terms of Roll Pitch and Yaw (RPY) angles, $\pm 1^\circ$ each. The worst combination of positive/negative angles produced a maximum error of about 2.5% nearly independent of the point location or $\boldsymbol{n}$ direction.

3.3. Inertial vs. body-fixed components

Some simulations have been carried out to evaluate the errors due to the assumptions that the linear acceleration components in the IRF are nearly equal to those in the BRF, as stated in Eq. (10). For an oscillation amplitude $\Theta = 1^\circ$ this error, with respect to the acceleration amplitude, is generally less than 1.5%. When Θ reaches 2°, the error grows proportionally to 3% and for smaller amplitudes $\Theta = 0.25^\circ$ it is reduced to 0.3%.

This evaluation can be verified by comparing non-diagonal and diagonal elements in the rotation matrix $R(t)$ in Eq. (19), the former being negligible with respect to the latter ones.

This error is almost independent of the rotation axis orientation (n) and the points coordinates.

In a real case the above-mentioned errors are present altogether, but it is not easy to assess whether their combination is worse than a single effect because they each can act differently on the three acceleration components.

An example of a simulated motion is reported in Fig. 2, for a test case with

- $\Theta = 1^\circ, \overline{\omega} = 4$ rad/s, $\psi = \pi/4$ rad in Eq. (17);
- $\alpha = -\pi/4$ rad $\beta = \pi/6$ rad in Eqs (18) and (19);
- accelerometer dimension $l = 10$ mm;
- $[O - \Omega]_B =$(2 l, 3 l, 2 l), so the distance of O from the rotation axis $\approx 4\, l$;
- $x_p = 4\, l$ and $y_Q = 5\, l$;
- $\pm 0.05\, l$ error in the location for both $[P - O]_B$ and $[Q - O]_B$;
- $\pm 1^\circ$ error in the orientation of the accelerometer axes, with the RPY approach.

The plotted results show the trend in a period of the dimensionless error of the acceleration components of P, obtained as the difference between the theoretical values and those calculated assuming the presence of errors, scaled by the modulus of the acceleration amplitude Eqs (8–9), i.e.

$$[err_P] = \frac{[\boldsymbol{a}_P(\text{theory})]_B - [\boldsymbol{a}_P(\text{errors})]_B}{|\overline{\boldsymbol{a}}_P|}. \tag{20}$$

In Fig. 2 different combinations of position and orientation errors are experienced by the three acceleration components: in the x and z directions the errors have opposite signs so they tend to balance one another, while in the y direction they sum up reaching 3%.

In order to verify the hypothesis of small vibrations, the dimensionless error due to the difference between IRF and BRF acceleration components

$$[err_P(IB)] = \frac{\boldsymbol{a}_P(\text{theory})]_I - [\boldsymbol{a}_P(\text{theory})]_B}{|\overline{\boldsymbol{a}}_P|}$$

is shown in Fig. 3.

A total error due to the combination of equipment errors (position and orientation of the accelerometer axes) and that related to the small vibration assumption

$$[err_P(tot)] = \frac{\boldsymbol{a}_P(\text{theory})]_I - [\boldsymbol{a}_P(\text{errors})]_B}{|\overline{\boldsymbol{a}}_P|}$$

is also reported.

It is interesting to underline that the error due to the change of reference system has twice the frequency of the body vibration but it affects second and higher order terms of small vibrations.

While the former two errors (position and orientation) can be reduced by an accurate experimental set up, the latter seems to be difficult to deal with, both in the experimental and in the processing stages.

The total error for the test case, which is not a favourable one with respect to the size of the errors introduced, keeps below 4%.

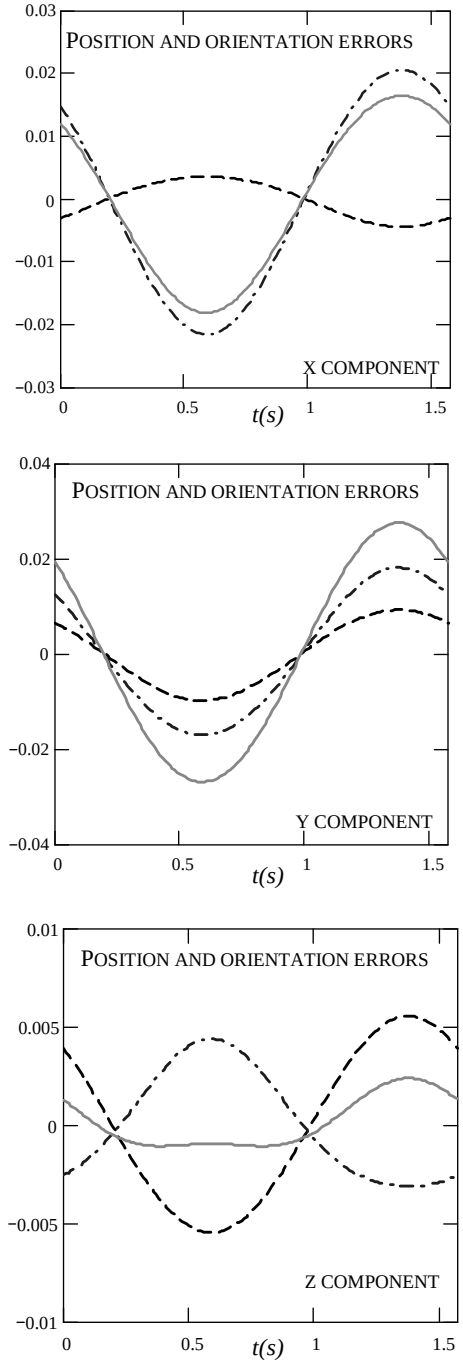

Fig. 2. Results of test case simulation: dimensionless errors [err_p]. Dashed line: position error; dadot line: orientation error; solid line combination of position and orientation errors.

3.4. Procedure simulation

The procedure proposed in §2.2 has first been simulated on the test case defined previously, assuming the presence of all the errors described in Fig. 3 and then verified experimentally (§4). Random noise has not been considered because it can be easily reduced with averaging techniques.

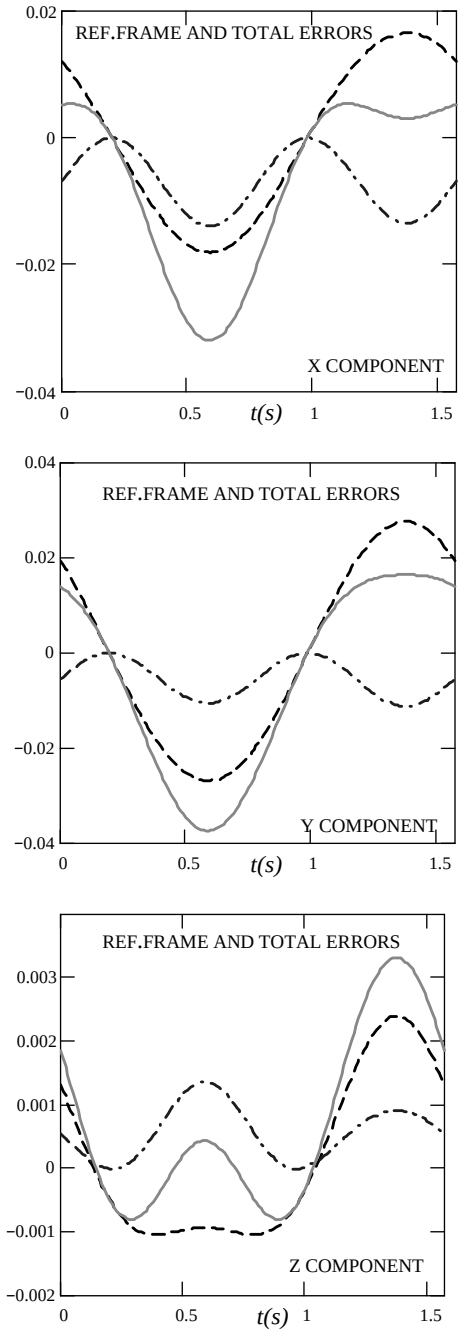

Fig. 3. Results of test case simulation: dimensionless errors. Dashed line: combination of position and orientation errors; dot-dashed line: $[err_p(IB)]$; solid line: total error $[err_p(tot)]$ combination of the previous ones.

The six accelerometer channels are supposed to acquire $a_{Ox}, a_{Oy}, a_{Oz}, a_{Py}, a_{Pz}, a_{Qz}$ in the BRF. The FFT of the data is rather simple since only one frequency is present; indeed second order effects can be observed. From amplitudes and phases the linear acceleration and velocity can be obtained according to Eqs (7–8) and, applying Eqs (11–16), also angular velocity and acceleration components can be calculated. In Figs 4 and 5 the dimensionless errors, that is the difference between theoretical and calculated values scaled by the amplitude, are reported, for angular velocity and acceleration respectively.

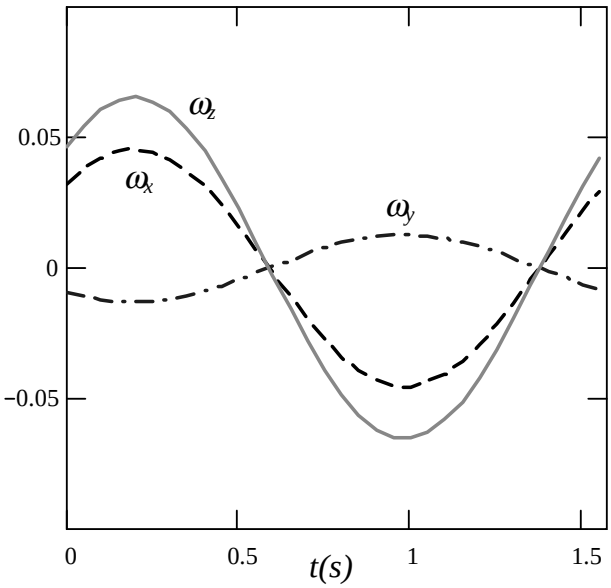

Fig. 4. Dimensionless angular velocity error $([\omega(\text{theoretical})] - [\omega(\text{calculated})]/\Theta\overline{\omega})$.

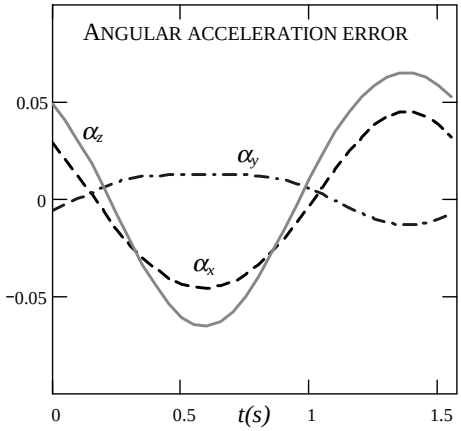

Fig. 5. Dimensionless angular velocity error $([\dot{\omega}(\text{theoretical})] - [\dot{\omega}(\text{calculated})]/\Theta\overline{\omega}^2)$.

As a result of the processing of accelerometric data, the errors increase up to 7%.

4. Experimental apparatus and testing

The proposed procedure has been experimentally validated and used to characterize the rigid motion of the hub connecting the steering wheel and the steering rod. To validate the procedure three additional channels were recorded, that is 9 acceleration components instead of 6. For this purpose three triaxial accelerometers, B&K 4326 A, were employed. Their main characteristics are: a charge sensitivity of 0.3 pC/ms $^{-2}$, frequency range of 27 kHz, 24 kHz and 48 kHz in the X, Y and Z directions respectively, resonance frequencies above 20 kHz, mass of 13 g.

The accelerometers, numbered 1, 2 and 3 in Fig. 6, were glued near the connection bolts of the steering wheel central plate and the hub. They were positioned so as to have their axes parallel to the BRF axes shown in Fig. 7.

During the tests all the acceleration components were acquired and recorded simultaneously.

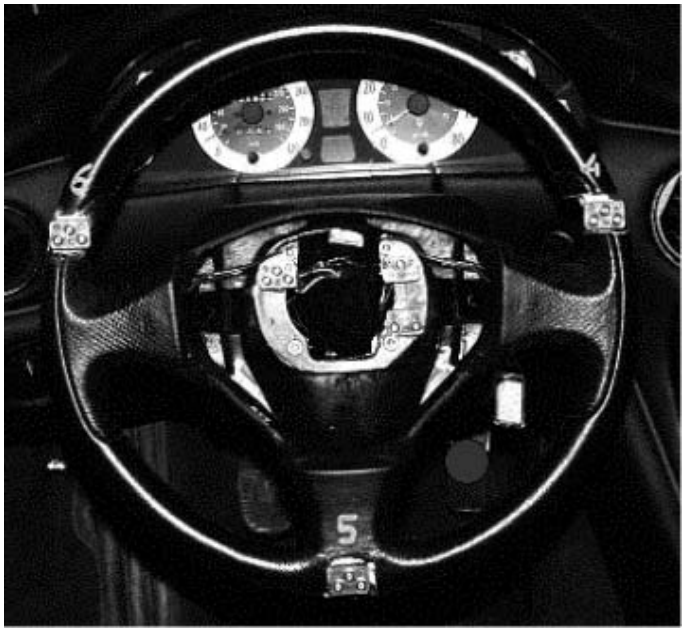

Fig. 6. Instrumented steering wheel.

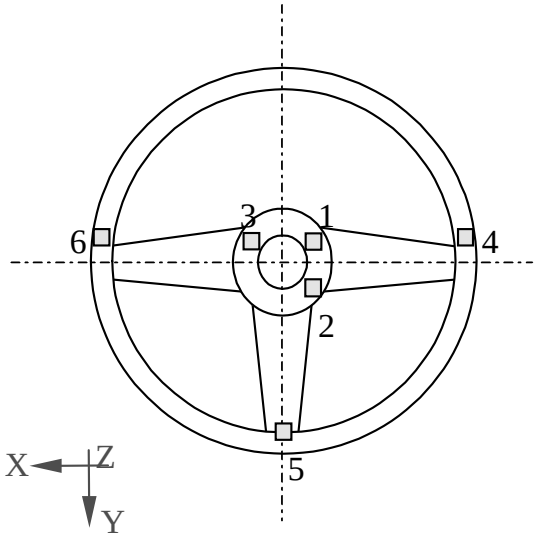

Fig. 7. Schematic of the steering wheel showing accelerometer positions and reference axes.

The acceleration signals were filtered by an anti-aliasing filter with a band width of 2 kHz. The sampling frequency was 5 kHz and each test recorded for 15 seconds.

The tests were carried out at constant vehicle speed, on a straight road, with the sixth gear engaged. Four different vehicle speeds were tested, ranging from 80 km/h up to 140 km/h, that is from 2095 to 3700 engine rpm. First the engine speed and the nine signals from the three accelerometers were recorded simultaneously in order to verify the hub rigid motion. Secondly only six components of the hub acceleration were recorded to fully describe its rigid body motion. In order to tune and validate a FE model of the steering wheel, by means of the known imposed vibration of the hub, three additional accelerometers (indicated as 4, 5 and 6 in Figs 6–7) were employed [1].

The experimental devices include a multi channel charge amplifier, B&K 5974, and a 24 channel Racal recorder.

Table 1
Amplitude and phase of the acceleration harmonic at 15 Hz measured by accelerometers 1, 2 and 3

	Amplitude $[m/s^2]$	Phase $[^\circ]$
ACC.1		
Direction X	0.58	167.07
Direction Y	0.19	81.07
Direction Z	0.13	20.84
ACC.2		
Direction X	0.61	165.31
Direction Y	0.19	82.22
Direction Z	0.2	0.51
ACC.3		
Direction X	0.63	164.58
Direction Y	0.19	66.72
Direction Z	0.19	10.23

Table 2
Calculated and experimental values of amplitude (in m/s^2) and phase (in degrees) of the harmonics corresponding to a_{2y}, a_{3x} e a_{3y} at 15 Hz

	Amplitude [m/s^2]	Phase$[^\circ]$
ACC.2-Y		
Calculated	0.19	81.2
Experimental	0.19	82.22
ACC.3-X		
Calculated	0.58	166.9
Experimental	0.63	164.58
ACC.3-Y		
Calculated	0.15	56.5
Experimental	0.19	66.72

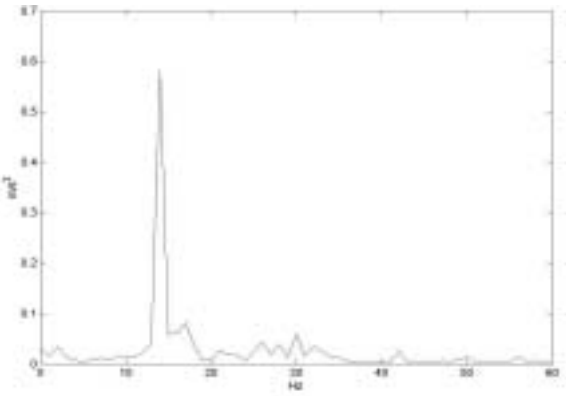

Fig. 8. Amplitude spectrum of acceleration in the X direction measured by accelerometer 1 (m/s^2).

The signals, expressed in g, were registered in a WAV format file, each 15 s long, then converted into TXT format files.

4.1. Data processing

The TXT files were imported in Matlab environment, whereby an FFT analysis of the acceleration spectra was obtained in terms of amplitude (in m/s^2) and of phase (in degrees), as shown in Figs 8–9.

Table 3
Percentage errors in the acceleration amplitudes and phases

Percentage errors	Amplitude	Phase
Accelerometer 2 Y direction	0.0	1.2
Accelerometer 3 X direction	7.9	1.4
Accelerometer 3 Y direction	21	15.3

Table 4
Normalised percentage errors in the acceleration amplitudes and phases

Percentage errors	E_A	E_ψ
Accelerometer 2 Y direction	0.0	0.56
Accelerometer 3 X direction	7.3	1.3
Accelerometer 3 Y direction	5.9	5.7

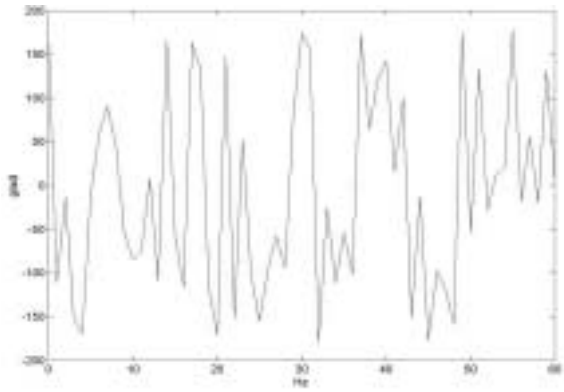

Fig. 9. Phase spectrum of acceleration in the X direction measured by accelerometer 1 (ℓ).

Since in the spectra by far the most important component in every direction is at 15 Hz, we decided to verify the hub rigid motion considering only the harmonic at that frequency.

The verification was carried out as follows: the acceleration components at 15 Hz corresponding to accelerometer 2 in the Y direction, a_{2y}, and to accelerometer 3 in the X and Y directions, a_{3x} e a_{3y}, were calculated by means of the procedure outlined in §2.2, i.e. by the accelerometer measurement of the other components. Then the calculated harmonics corresponding to a_{2y}, a_{3x} e a_{3y} at 15 Hz were compared to those measured by the accelerometers.

4.2. Results

In Table 2 the calculated and experimental values are reported.

The percentage errors of the calculated amplitudes and phases compared to the experimental ones are reported in Table 3.

It is also interesting to evaluate the amplitude errors relating them to the modulus of the measured amplitude vector, by means of the formula

$$E_A = \frac{|A_{\text{exp}} - A_{\text{calc}}|}{|A|} 100.$$

As far as the phase error is concerned, it can be related to the maximum phase, 180 °, by means of the formula

$$E_\psi = \left| \frac{\psi_S - \psi_C}{180} 100 \right|.$$

The errors E_A and E_ψ described above are summarized in Table 4.

Considering the small absolute values of amplitude, the agreement of the experimental values and those calculated by the formulas of the rigid body motion is satisfactory, especially if we consider harmonic a_{2y}. Moreover the errors of harmonics a_{3x} and a_{3y} appear acceptable considering the errors in the alignment of the accelerometer axes and in the measurement of the distances between the accelerometers, d_{12} and d_{13}, measurement noise and errors due for example to the accelerometer mounting system and to their transverse sensitivity. Therefore we can state that six acceleration components are sufficient to define the rigid body motion of the hub of the steering wheel.

5. Conclusions

A simplified procedure for the identification of the 3D vibratory motion of a rigid body by accelerometer measurements has been developed and validated.

The outlined procedure appears particularly convenient for bodies not easy to handle or to modify for instrumentation.

It has been shown both analytically and experimentally that in the case of vibratory motion, i.e. for small oscillations, six accelerometers are sufficient to define the rigid body motion and FFT can be conveniently used to avoid time integration of signals and consequent accumulation of errors.

Numerical simulation has been used to evaluate the significance of set-up and measurement errors.

References

[1] C. Carmignani et al., *Studio numerico e sperimentale del comportamento dinamico di un volante*, XVI Congresso Aimeta, Ferrara, Italy, CD, 2003, pp.1–10.

[2] Y.K. liu, Discussion on measurement of angular acceleration of a rigid body using linear accelerometers, *ASME Journal of Applied Mechanics* **43** (1976), 977–978, Author's closure, p. 378.

[3] N.K. Mital and A.I. King, Computation of rigid-body rotation in three-dimensional space from body-fixed linear acceleration measurements, *ASME Journal of applied Mechanics* **46** (1979), 925–930.

[4] A.J. Padgaonkar, K.W. Krieger and A.I. King, Measurement of angular acceleration of a rigid body using linear accelerometers, *ASME Journal of Applied Mechanics* **42** (1975), 552–556.

[5] B. Zappa, G. Legnani and R. Adamini, *Posizionamento ottimo e calibrazione di sensori per misure accelerometriche in 3D*, XV Congresso AIMETA, Taormina, Italy, CD, 2001, pp. 1–10.

[6] B. Zappa, G. Legnani, A.J. van den Bogert and R. Adamini, On the number and placement of accelerometers for angular velocity and acceleration determination, *ASME Journal of Dynamic Systems, Measurement, and Control* **123** (2001), 552–554.